PIN WITHOUT HEAD HR-18152 - TIN BRONZE - LATE BRONZE AGE - SWITZERLAND

Artefact name Pin without head HR-18152

Authors Marianne. Senn (EMPA, Dübendorf, Zurich, Switzerland) & Christian. Degrigny (HE-Arc CR, Neuchâtel, Neuchâtel, Switzerland)

Url /artefacts/217/

The object

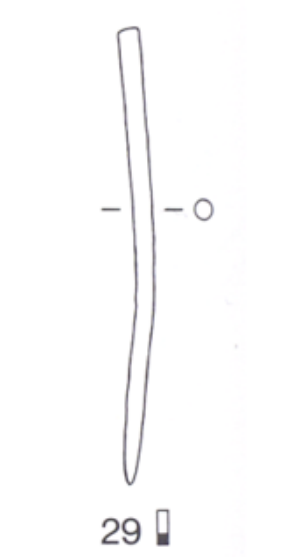

Credit HE-Arc CR.

Fig. 1: Tin bronze pin without head (after Rychner-Faraggi 1993, plate 74.29),

Description and visual observation

Description of the artefact	Pin without head, light-brown patina typical of lake context. Dimensions: L = 7,5cm; Ø = 3.3mm; WT = 4g.
Type of artefact	Pin
Origin	Hauterive - Champréveyres, Neuchâtel, Neuchâtel, Switzerland
Recovering date	Excavation 1983-1985, object from layer 3 to 5
Chronology category	Late Bronze Age
chronology tpq	1054 B.C.
chronology taq	1000 B.C.
Chronology comment	Hallstatt B1 (1054/1037BC _ 1000BC)
Burial conditions / environment	Lake

Artefact location	Laténium, Neuchâtel, Neuchâtel
Owner	Laténium, Neuchâtel, Neuchâtel
Inv. number	Hr 18152
Recorded conservation data	Not conserved

Study area(s)

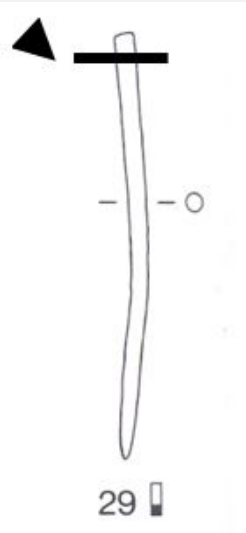

Credit HE-Arc CR.

Fig. 2: Location of sampling area,

Binocular observation and representation of the corrosion structure

Stratigraphic representation: none

MiCorr stratigraphy(ies) – Bi

Sample(s)

Fig. 3: Micrograph of the cross-section showing the locations of Figures 4 to 11,

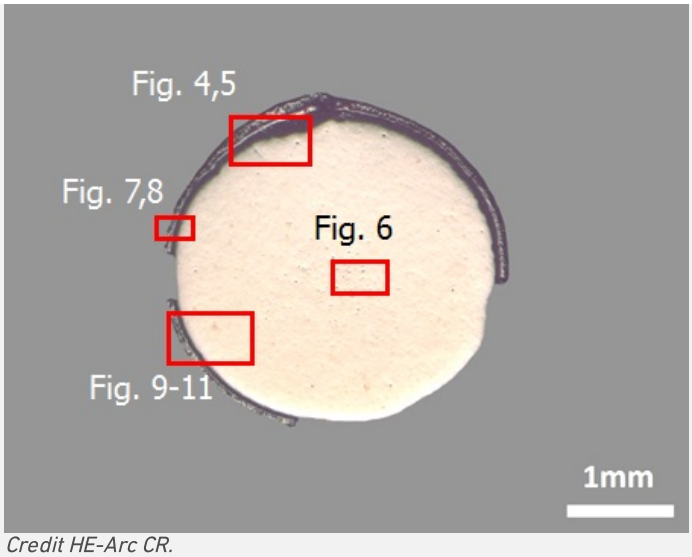

Credit HE-Arc CR.

Description of sample	The cross-section is circular and is a complete section through the pin (Figs. 2-3). It is covered with a rather thin and regular (in thickness) corrosion crust. One third of the corrosion crust is missing.
Alloy	Tin Bronze
Technology	Annealed after cold working
Lab number of sample	MAH 87-194
Sample location	Musées d'art et d'histoire, Genève, Geneva
Responsible institution	Musées d'art et d'histoire, Genève, Geneva
Date and aim of sampling	1987, metallography and corrosion characterisation

Analyses and results

Analyses performed:
Metallography (etched with ferric chloride reagent), Vickers hardness testing, XRF, ICP-OES, SEM/EDX, XRD, Raman spectroscopy.

Non invasive analysis

Metal

The remaining metal is a tin bronze and contains copper sulphide as well as heavy metal (Pb-rich) inclusions (Table 1, Figs. 4 and 5). Close to the surface of the remaining metal, copper sulphide inclusions are elongated and form rows (Fig. 4). The etched structure of the tin bronze shows polygonal grains; some of them are twinned (Fig. 6). In the centre of the sample and on the side, the grains are smaller. The copper sulphide inclusions are located at the grain boundaries and in the grains. The average hardness of the metal is about HV1 110.

Elements	Cu	Sn	Pb	Sb	As	Ag	Fe	Ni	Co	Zn
mass%	89.22	9.57	0.34	0.26	0.19	0.15	0.09	0.05	0.06	0.05

Table 1: Chemical composition of the metal. Method of analysis: ICP-OES, Laboratory of Analytical Chemistry, Empa.

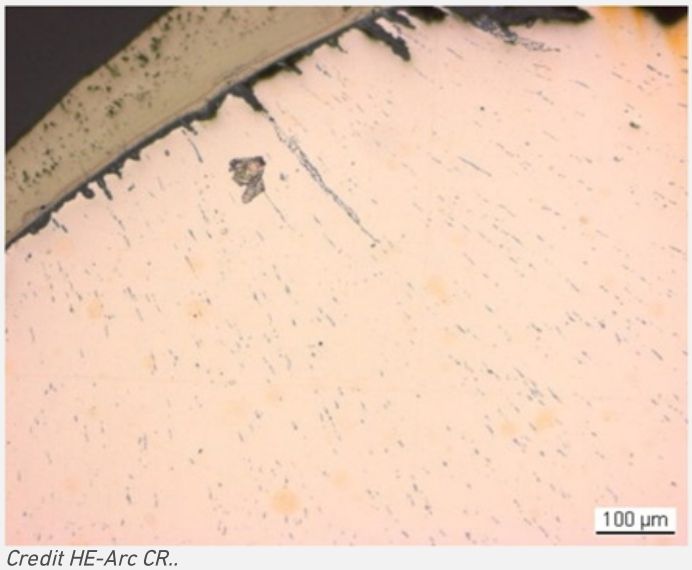

Credit HE-Arc CR..

Fig. 4: Micrograph of the metal sample from Fig. 3 (detail), unetched, bright field. Rows of elongated copper sulphide inclusions can be observed,

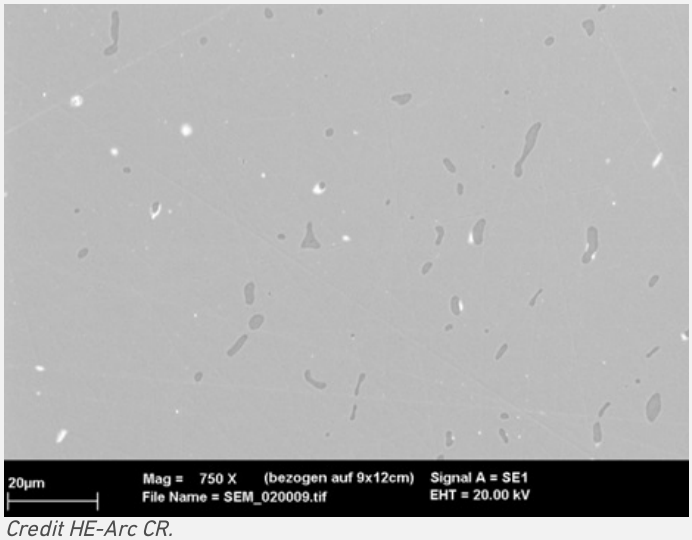

Credit HE-Arc CR.

Fig. 5: SEM image of the metal sample from Fig. 3 (detail), SE-mode. Elongated copper sulphide inclusions (dark-grey) are visible as well as heavy metal (Pb-rich) inclusions (white),

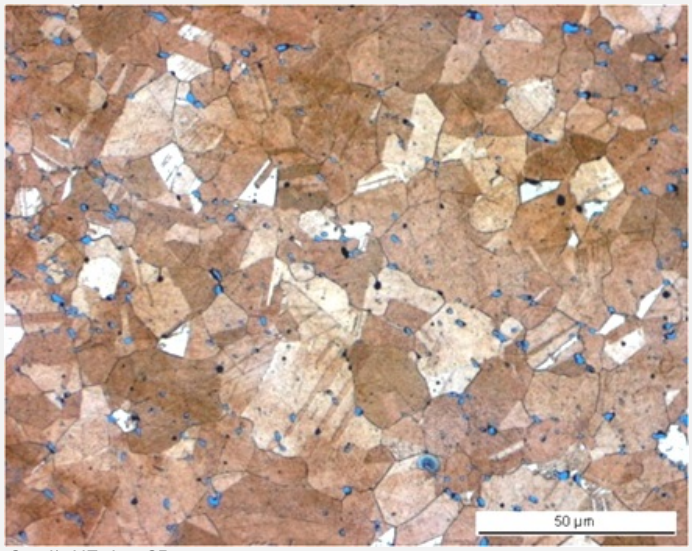

Credit HE-Arc CR.

Fig. 6: Micrograph of the metal sample from Fig. 3 (detail), etched, bright field. The metal shows a structure of polygonal and twinned grains. Copper sulphide inclusions are visible as blue spots,

Microstructure	Polygonal and twinned grains
First metal element	Cu
Other metal elements	Sn

Corrosion layers

The corrosion crust is regular in thickness (100µm). One third is missing (Fig. 3). At the metal - corrosion crust interface, there is a crack showing that the latter has separated from the metal core along its whole length (Figs. 7 and 8). The corrosion crust can be divided into three distinct layers. Directly above the crack is a first dense but cracked and irregular inner layer (Figs. 7 and 8). In bright field it appears brown (Fig. 9), in polarised light dark (Fig. 10). It is separated from the adjacent layer by a clear line (Figs. 8 and 9). The second layer is dense with little porosity (Figs. 7 and 8). In bright field it appears light-brown (fig. 9), in polarised light-black (Fig. 10). The third and outermost layer (light-brown in bright field, Fig. 9) contains particles (Fig. 8) and is very porous (appearing as golden reflections under polarized light, Fig. 10). The elemental chemical distribution of the SEM image selected reveals that the inner layer is depleted in Cu but Sn,O and Si-rich (Fig. 11 and Table 2) and its interface with the intermediate layer could represent the limit of the original surface (Figs. 7 and 11). The second and third layers are Fe,Cu and S-rich (Fig. 11) and have a composition similar to chalcopyrite/$CuFeS_2$ (Table 2). This was confirmed by XRD. The particles (inclusions) have a composition similar to covelline/CuS (Table 2). Both chalcopyrite and covelline have been identified by Raman spectroscopy (Figs. 12 and 13).

Elements	S	Fe	Cu	O	Si	Sn	Total
CP1e and CP2i	35	30	34	<	<	<	99
Particles in CP1e	26	4.1	68	<	<	<	98
CP3i	5.8	5.0	13	32	2	41	99

Table 2: Chemical composition (mass %) of the corrosion layer from Fig. 9. Method of analysis: SEM/EDX, Laboratory of Analytical Chemistry, Empa.

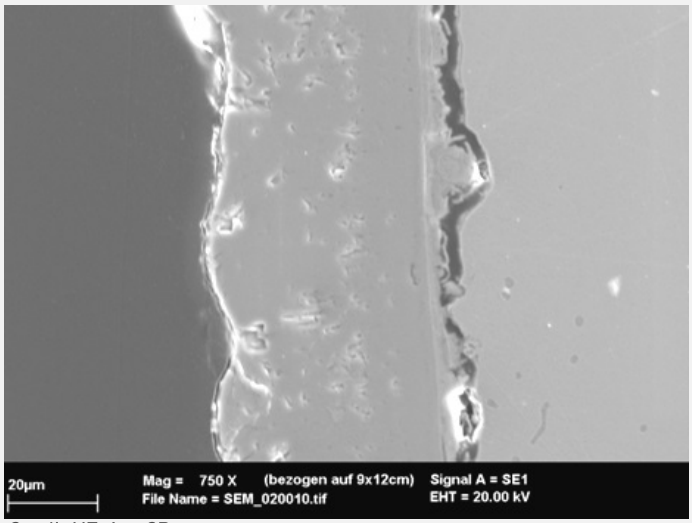

Credit HE-Arc CR.

Fig. 7: SEM image of the metal sample from Fig. 3 (detail), SE -mode. The crack between the remaining metal and the corrosion layers is clearly visible,

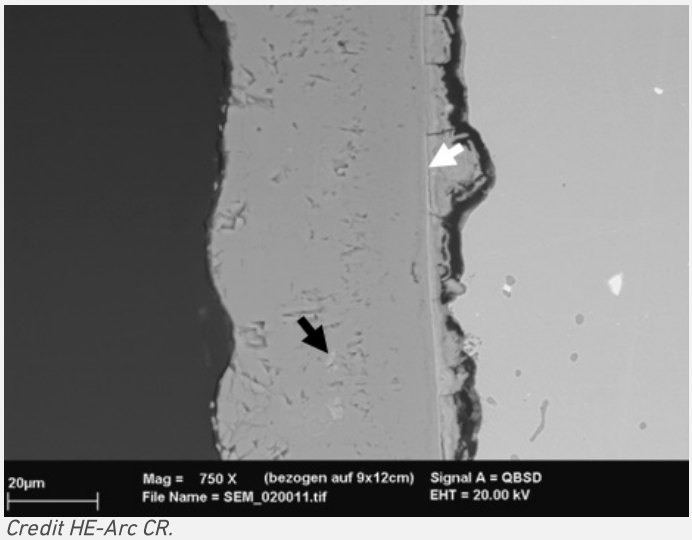

Credit HE-Arc CR.

Fig. 8: SEM image similar to Fig. 7, BSD -mode. A thin line is visible (white arrow) differentiating the inner Sn-rich layer from the intermediate and outer chalcopyrite layers. The latter contains bright covelline inclusions (black arrow) and pores,

Fig. 9: Micrograph of the metal sample from Fig. 3 (detail), unetched, bright field,

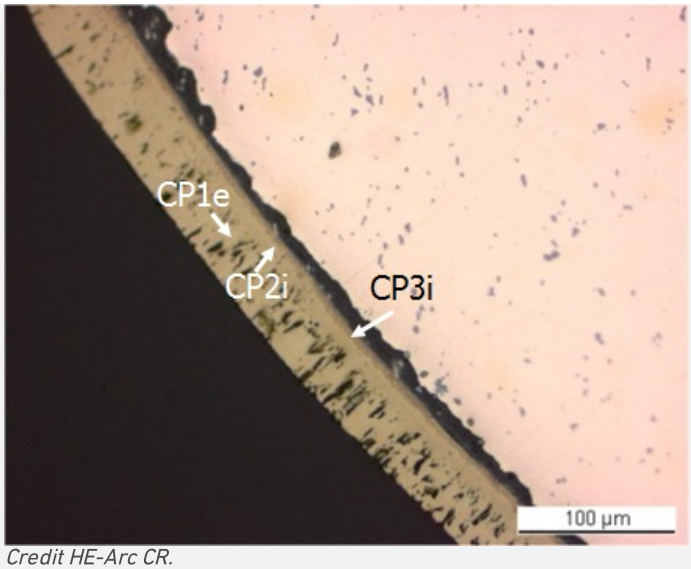

Credit HE-Arc CR.

Fig. 10: Micrograph similar to Fig. 9, polarised light,

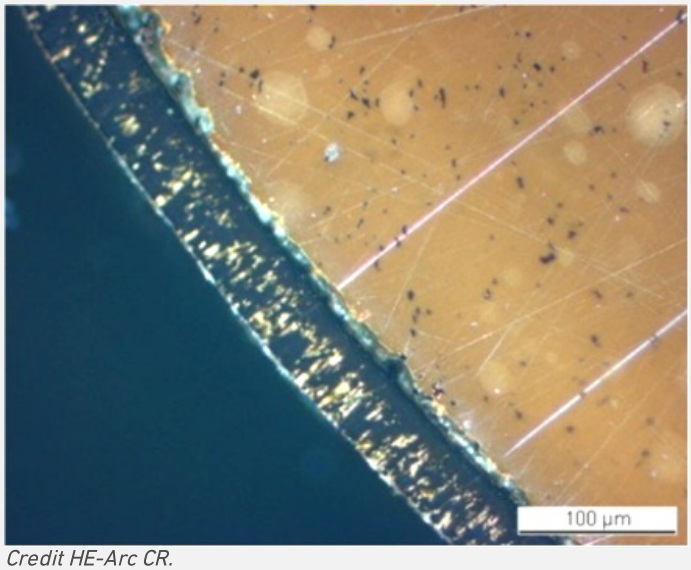

Credit HE-Arc CR.

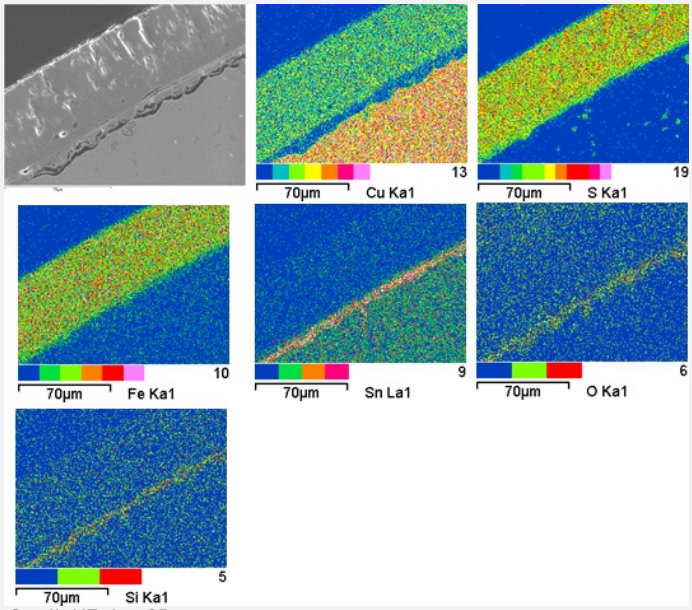

Credit HE-Arc CR.

Fig. 11: SEM image and elemental chemical distribution of a selected area of Fig. 9 (rotated by 90°). Method of examination: SEM/EDX, Laboratory of Analytical Chemistry, Empa,

Fig. 12: Raman spectrum of the outermost layer (S23) of Fig. 10 compared to a chalcopyrite standard spectrum. Settings: laser wavelength 532nm, acquisition time 50s, 4 accumulations, filter D2 (0.75-0.8mW), hole 1000, slit 100, grating 600. Method of analysis: Raman spectroscopy, Lab of Swiss National Museum, Affoltern a. Albis ZH,

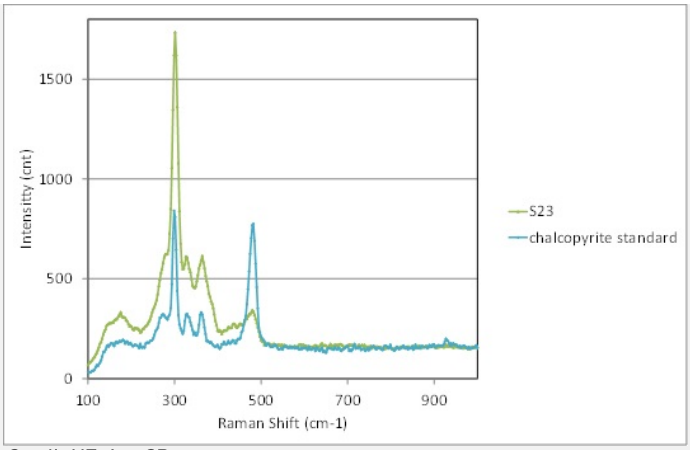

Credit HE-Arc CR.

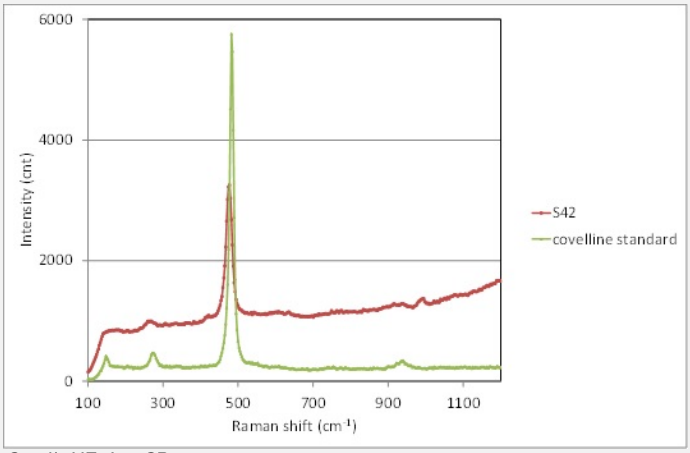

Credit HE-Arc CR.

Fig. 13: Raman spectrum of the outermost layer (S42) of Fig. 10 compared to a covelline standard spectrum. Settings: laser wavelength 532nm, acquisition time 10s, 5 accumulations, D2 (0.75-0.8mW), hole 500, slit 80, grating 600. Method of analysis: Raman spectroscopy, Lab of Swiss National Museum, Affoltern a. Albis ZH,

Corrosion form	Uniform - pitting
Corrosion type	Type I (Robbiola)

MiCorr stratigraphy(ies) – CS

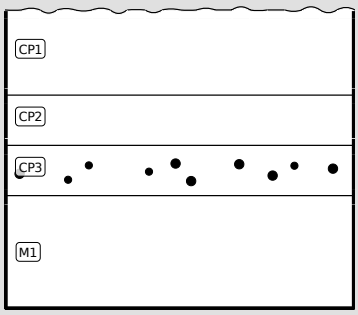

Fig. 4: Stratigraphic representation of the object in cross-section using the MiCorr application. This representation can be compared to Fig. 10.

Synthesis of the binocular / cross-section examination of the corrosion structure

Corrected stratigraphic representation: none

Conclusion

The pin is made from tin bronze and has been annealed after cold working. It is covered with a regular, light-brown patina typical of lake context (Schweizer 1994). The inner, thin Sn-rich corrosion layer contains soil elements such as Si. The light-brown, thick intermediate and outer corrosion layers have the composition of chalcopyrite. This object was certainly abandoned rather quickly in an anaerobic, humid and S and Fe-rich environment, favouring then the formation of chalcopyrite. The limit of the original surface can be located between the chalcopyrite and the Cu depleted but Sn-rich inner corrosion layer. Thus, the corrosion is a type 1 according to Robbiola et al. 1998.

References

References on object and sample

References object

1. Rychner-Faraggi A-M. (1993) Hauterive – Champréveyres 9. Métal et parure au Bronze final. Archéologie neuchâteloise, 17 (Neuchâtel).
2. Hochuli, S. et al. (1988) SPM III Bronzezeit , Verlag Schweizerische Gesellschaft für Ur- und Frühgschichte Basel, 76-77, 379.

References sample

3. Empa Report 137 695/1991, P.O. Boll.
4. Rapport d'examen, Lab. Musées d'Art et d'Histoire, Geneva GE, 87-194 à 87-197.
5. Schweizer, F. (1994) Objets en bronze provenant de sites lacustre: de leur patine à leur biographie. In: L'œuvre d'art sous le regard des sciences (éd. Rinuy, A. and Schweizer, F.), 143-157.

References on analytic methods and interpretation

6. Robbiola, L., Blengino, J-M., Fiaud, C. (1998) Morphology and mechanisms of formation of natural patinas on archaeological Cu-Sn alloys, Corrosion Science, 40, 12, 2083-2111.